SPACECRAFT CHARGE BUILDUP ANALYSIS

NATIONAL AERONAUTICS AND SPACE ADMINISTRATION

NASA SP-276

SPACECRAFT CHARGE BUILDUP ANALYSIS

by

William S. West
Goddard Space Flight Center

J. V. Gore and M. A. Kasha
RCA Research Laboratories

and

Herbert W. Bilsky
RCA Astro-Electronics Division

Prepared at NASA Goddard Space Flight Center

Scientific and Technical Information Office 1971
NATIONAL AERONAUTICS AND SPACE ADMINISTRATION
Washington, D.C.

For sale by the National Technical Information Service
Springfield, Va. 22151
Price $3.00
Library of Congress Catalog Card Number 78-172496

FOREWORD

During the past several years, missions to the vicinity of Jupiter and beyond have received considerable attention, because of the unique alignment of the outer planets. The alignment, which will not occur again for 175 years, will allow spacecraft missions to these regions with relatively modest launch energies.

Accuracy of measurement of certain scientific instruments useful for deep-space missions can be altered significantly by the presence of an ambient-to-spacecraft electrical potential. The magnitude of this potential depends on the spacecraft's immediate environment. Accordingly, estimates of the potential in various environments are given here for a typical deep-space trajectory.

The information provided is timely and merits consideration because of the current opportunities for exploration.

Page intentionally left blank

CONTENTS

Section		*Page*
	Foreword	iii
	GLOSSARY OF SYMBOLS	vii
I	INTRODUCTION	1
II	ANALYSIS OF THE CHARGED-PARTICLE ENVIRONMENT	9
	A. Charge Buildup Mechanism–Brief Description	9
	B. The Space Environment	9
	C. Other Charging Sources (Excluding RTG's)	17
	D. Radiation Environment Induced by RTG's	18
III	CURRENT DENSITY FROM VARIOUS SOURCES	21
IV	SPACECRAFT FLOATING POTENTIAL	23
	A. Charge Potential Equations	23
	B. Spacecraft Potential	25
V	PROTECTIVE MEASURES RECOMMENDED FOR CHARGE BUILDUP PROBLEM AREAS	29
VI	CONCLUSIONS	31
	ACKNOWLEDGMENTS	33
	References	35

Page intentionally left blank

GLOSSARY OF SYMBOLS

A	Correction factor for restricting electron collection in a magnetic field
B	Magnetic field
B_0	Equatorial magnetic field of Jupiter
E	Particle energy
E_i	Ion energy
e	Electron charge
$f(E_i)$	Ion energy spectrum
I_e	Electron current
I_i	Ion current
I_{ph}	Photoelectric current
i_{ph}	Photoelectric current density
i_r	Total current density to the body by one component
k	Boltzmann's constant
M	Ion mass
m	Electron mass
n	Electron (and ion) density
n_e	Electron density
n_i	Ion density
R_e	Earth radii
R_j	Jupiter radii
r	Radius of the sphere (model of spacecraft)

r_s	Distance from Sun
T_e	Electron temperature
T_i	Ion temperature
T_{ph}	Photoelectron temperature
V_f	Floating potential
v_0	Spacecraft velocity
v_0'	Spacecraft velocity in nonrotating frame
$\delta(E_i)$	Secondary electron yield
$\delta_{i,e}$	Secondary emission coefficient for ions or electrons
ϕ	Potential
Φ_e	Electron flux
Φ_i	Ion flux
ΩR_j	Particle velocity relative to spacecraft (near-Jupiter region)

SPACECRAFT CHARGE BUILDUP ANALYSIS

by

William S. West
Goddard Space Flight Center

J. V. Gore and M. A. Kasha
RCA Research Laboratories

and

Herbert W. Bilsky
RCA Astro-Electronics Division

SECTION I

INTRODUCTION

Since the early 1960's, personnel of the Goddard Space Flight Center (GSFC) have been interested in deep-space missions to obtain information concerning the planets Jupiter, Saturn, Uranus, Neptune, and Pluto, as well as information concerning the interplanetary medium. Studies have been performed to establish the feasibility of such missions and various reports were written by GSFC personnel and by others.

For almost as long as these missions have been considered, the engineers, scientists, and managers at GSFC have realized the necessity for systems, independent of the Sun's energy, to meet the spacecraft electric power requirement. In general, GSFC studies have indicated that there is a weight advantage in using small nuclear power systems such as radioisotope fueled thermoelectric generators (RTG's) instead of presently available solar cells when missions go beyond 2.5 or 3 AU. Further, there are technological and practical uncertainties in projecting use of solar arrays in a range starting beyond 3-5 AU*, whereas the use of small nuclear power supplies is technically feasible. However, the use of small nuclear systems, while practical, nevertheless presents technical questions. An in-house GSFC study identified pertinent technological areas requiring study prior to the use of these nuclear

*Technical uncertainties involve practical design questions arising from the use of very large solar array areas, their survival through meteoroid belts, and their system performance when operating at the low temperature and low illumination levels anticipated. This topic is also discussed in studies by J. Epstein, W. S. West, and W. D. Harris on advanced nuclear systems.

generators on spacecraft designed for scientific deep-space missions. These areas were divided into the following numbered tasks:

Task Number	Task Description–Title	Reference Document
I	Analysis of Selected Deep-Space Missions	~
IIA	Subsystem Radiation Susceptibility Analysis of Deep-Space Missions	~
IIB	Spacecraft Charge Buildup Analysis	~
III	Techniques for Achieving Magnetic Cleanliness	~
IV	Weight Minimization Analysis	X-701-69-174*
V	Spacecraft Analysis and Design	X-701-69-175*
VI	Spacecraft Test Documentation	X-701-69-176*
VIIA	Planar RTG-Component Feasibility Study	X-701-69-177*
VIIB	Planar RTG-Spacecraft Feasibility Study	X-701-69-178*
VIII	RTG Interface Specification	TM X-63617
~	Summary Report of NEW MOONS	X-701-69-190*

*Goddard Space Flight Center unpublished report.

A contract** was established for further study of these areas. This study was entitled NASA Evaluation With Models Of Optimized Nuclear Spacecraft (NEW MOONS). During the execution of the NEW MOONS technology study, GSFC was assigned the task of conducting a Phase A study covering a Galactic Jupiter Probe. These two study efforts, Galactic Jupiter Probe (GJP) and NEW MOONS, were directed to provide the maximum practical benefit to each other. In general, the GJP was considered as a "baseline spacecraft and mission" or a "reference design" during the NEW MOONS technology study. On the other hand, the GJP Study team made use of the technology and data as developed by the NEW MOONS Study in areas of missions analysis, shielding, aerospace nuclear safety, thermal and structural analysis, and other related areas.

As the NEW MOONS contract was being concluded, the scope of the Galactic Jupiter Probe project was broadened and adopted the name Outer Planets Explorer (OPE). The OPE is considered for a generally more ambitious program than the original GJP, in that the OPE is intended for a family of single- and multiple-planet missions.

The OPE, as presently visualized, encompasses spacecraft in the 1100- to 1400-pound class, whereas the GJP "reference-design spacecraft" for the NEW MOONS Study was 500 to 600 pounds. This is a significant practical difference from a flight project viewpoint; however, the technology and techniques of NEW MOONS are generally applicable. Specific numeric values will be different when solutions are developed, but the techniques and rationale indicated in the NEW MOONS reports are applicable to the general problem of integrating and using small nuclear power systems on a scientific

**NAS 5-10441 RCA Astro-Electronics Division, Princeton, N.J. RCA Research Laboratories, Montreal, Canada, supported RCA Astro-Electronics Division in performing portions of the charge buildup study.

spacecraft designed for deep-space missions. The NEW MOONS technology and techniques reported may have applicability or some relevancy to additional space missions such as planetary landers and rovers as well as applications spacecraft that may in the future use nuclear systems.

The subject of charge buildup on a body in space had been considered for some 25 years prior to the advent of Earth-orbiting satellites. One of the first papers to discuss the subject of the equilibrium of electric charge appeared in 1937.* This paper treated positive-ion and electron collection and photoemission. Other papers subsequently appeared, extending and refining the analysis. In 1956, Lehnert** applied analysis to a postulated Earth orbiter. A few years later Sputnik 3 actually measured spacecraft charge and indicated a negative potential varying from −2 to −7 volts with altitude and with day-night conditions. Other papers appeared later, continuing the process of analytical refinement but with the additon of measurements provided from Earth orbiters and rocket flights. In particular, Reference 1 indicates that "a body in the upper atmosphere or in space will acquire an electric charge, or potential, which must be known ... to assess the behavior of certain experiments on satellites" and that "(radioactive) material in a body in space constitutes a charging mechanism .... Satellites sometimes carry quantities of radioactive material in conjunction with certain types of experiments, or as a power source. Such sources are normally well shielded but should still be considered as potential charging mechanisms. Clearly, each such source must be evaluated individually." It can be seen that this subject has received considerable study over the years and is in a continuing state of re-evaluation as new measurements are made and new theories are proposed.

It is interesting to note the developing picture of the Earth's magnetic field, which is associated with the subject of charge buildup, brought about by space-age observations. A dramatic comparison of old and new viewpoints is shown in Figure 1.

The Task I missions analysis report indicates the necessity for RTG's for the mission into deep space. Task IIB, therefore, examines briefly the literature and current project plans and postulates the spacecraft potential that might be expected by the Galactic Jupiter Probe or Outer Planet Explorer. The variation in the naturally occurring discharging mechanisms is also considered.

The purpose of Task IIB was to consider and estimate the extent of charge buildup for a deep-space spacecraft due to the RTG and the space environment and the effect that this estimated charge buildup would have on the spacecraft subsystems. For this Task, the Galactic Jupiter Probe spacecraft† described by the Task V effort and in the Galactic Jupiter Probe Study has been selected as the baseline configuration. A 1/18 scale model of this spacecraft is shown in Figure 2. The analytical techniques used in this report are somewhat independent of the baseline spacecraft configuration selected, and the techniques are generally applicable to any deep-space mission or spacecraft configuration. It will be shown that effects due to the RTG's are negligible in the cases studied; however, the effects due to the space environment, particularly with respect to experimental sensors, merit consideration.

*Jung, B. *Astron. Nach.* 263(1937):426.

**Lehnert, B. *Tellus* 8(1956):408.

†The spacecraft weight is approximately 600 lb, and its two RTG's each contain approximately 1725 watts (thermal) of PuO_2 fuel.

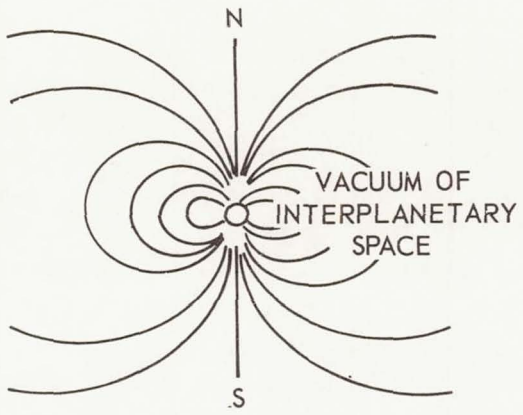

A. Simple dipole model of Earth's magnetic field, representing earlier understanding.

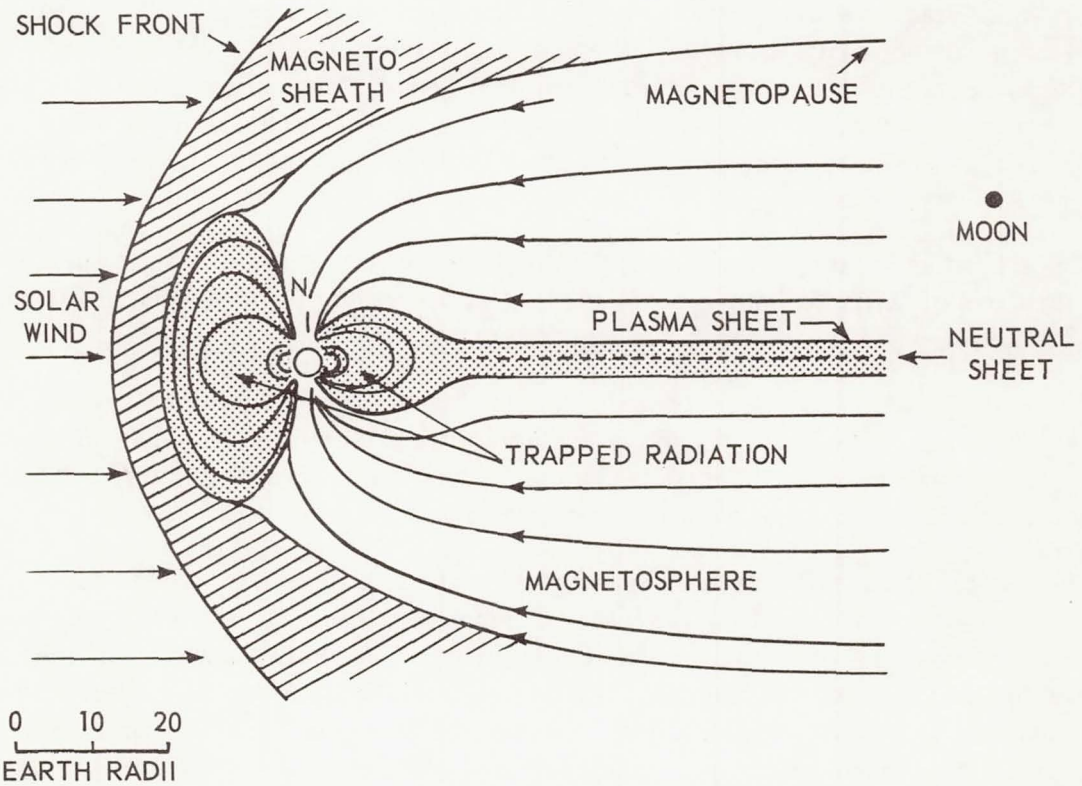

B. "Doughnut and tail" model of Earth's magnetic field, representing present concepts after a decade of spacecraft observations. Dot marked "Moon" indicates relative distance at which the Moon's orbit intersects plane of view. View plane contains Sun-Earth line and geomagnetic axis.

Figure 1—Earth's magnetic field.*

**Physics of the Earth in Space*, October 1968. A report of a study by the Space Science Board, Woods Hole, Massachusetts, National Academy of Sciences.

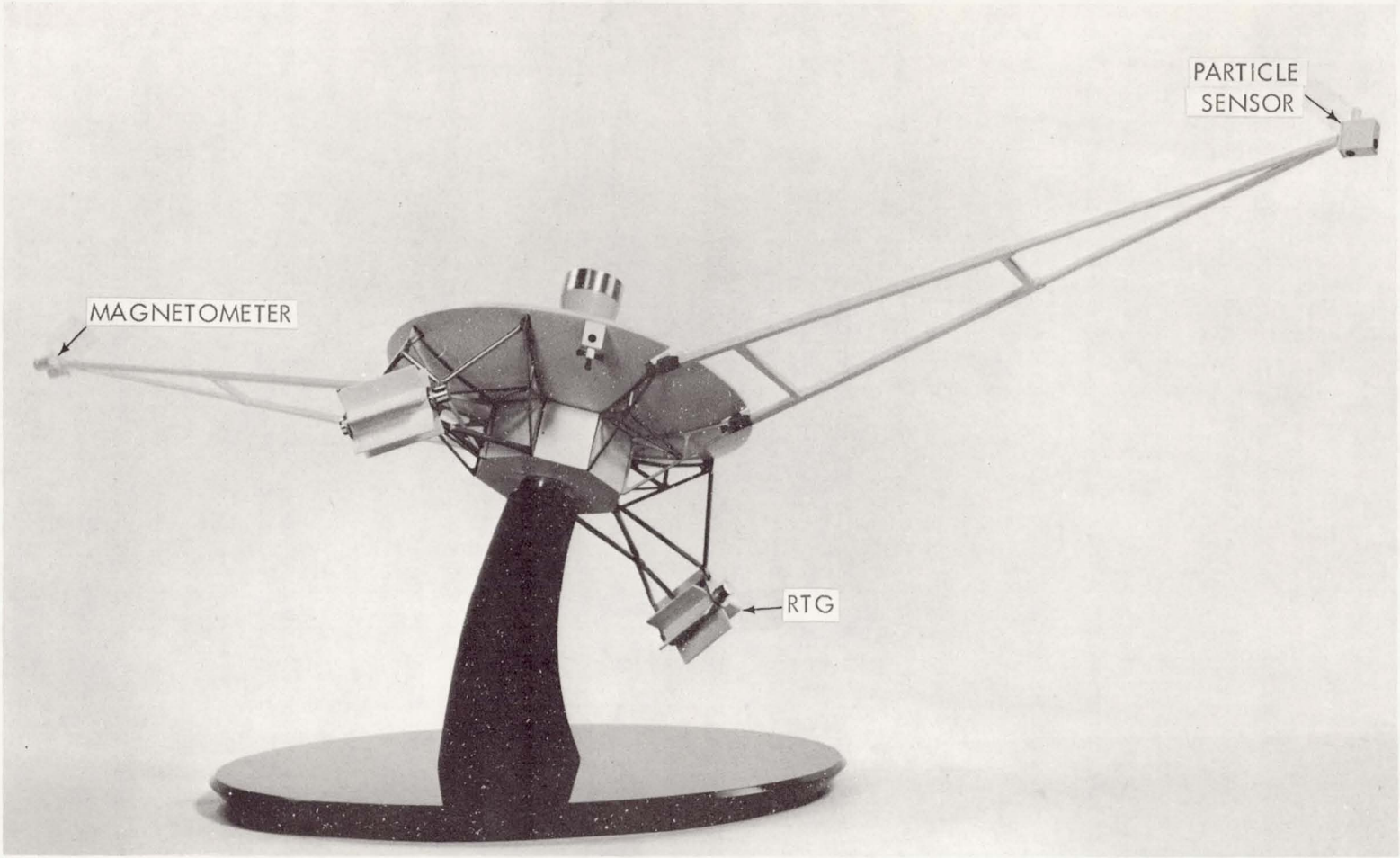

Figure 2—Model of the Galactic Jupiter Probe.

As the spacecraft travels along its flight path from Earth to the regions of Jupiter and beyond, it will be constantly bombarded by charged particles, principally electrons, positive ions, protons, and also photons, causing an accumulation of charge on the spacecraft. The rate of flow of positively and negatively charged particles to and from the surface of the spacecraft determines its equilibrium, or floating, potential. Equilibrium potential is established when the total current entering or leaving the spacecraft is zero. In a plasma with an equal number of electrons and positive ions at approximately the same particle temperature, the equilibrium potential of a conducting surface will be slightly negative because the higher electron velocity produces a greater electron flux. If protons are present in much larger quantities, the result will be a positive equilibrium potential. Photoelectrons generated by the effect of sunlight on the spacecraft surface can also alter the floating potential, tending to make it more positive; secondary emission from bombarding electrons would have a similar effect.

In evaluating the natural sources of charge buildup, the regions of near-Earth, interplanetary space, and near-Jupiter will be considered separately; the particle effects that are not limited to a particular region, such as photoemission and secondary emission, are also considered. The spacecraft potential resulting from these sources of charge buildup for various regions of space is estimated, and possible measures for avoiding difficulties from charge buildup effects are recommended.

In interplanetary space, the charge-discharge mechanisms may be significantly altered from the models assumed in this report. If one postulates pockets of extremely low charged-particle density, or "voids," then the charge buildup due to onboard RTG's may become relatively more significant than is indicated by the models used in this report. This report does not specifically cover the considerations associated with charged particles originating outside the solar system. They too may significantly alter the charge-discharge mechanism.

This report discusses the mechanism of spacecraft charge buildup and the resulting equilibrium floating potential on a selected deep-space spacecraft in the various environments to be encountered. The parameters of the relevant regions of space are presented, and, where experimental data are available, the representative values and their range are indicated. Where no datum exists, the values of the parameters are based on the models by several authors. As a result, data on the near-Jupiter region are speculative, and wide excursions from the given numbers are probable. Similarly, data for the region of interplanetary space beyond Jupiter to 10 AU are speculative; extrapolation to this region is based on data from the 1 to 1.5 AU area. Those regions of space beyond 10 AU or out of the ecliptic plane are not studied.*

Equations for charge collection from the major charge sources as a function of body potential are used to develop approximate equations for the equilibrium floating potential of a spherical body, the model for the spacecraft. The major sources of charge are (1) electrons and ions from the thermal plasmas, (2) high energy particles, (3) secondaries produced as a result of particle impact, and (4) photoelectrons. In addition to these major sources, the RTG's contribution to the charging mechanism is considered. Near Earth, the flux of electrons and protons is at least two orders of magnitude less than the flux of thermal electrons and photoelectrons. In the region of Jupiter's proton radiation belt,

*For a description of the uncertainties of deep-space and out-of-the-ecliptic regions see *Physics of the Earth in Space*, October 1968. A report of a study by the Space Science Board, Woods Hole, Mass., National Academy of Sciences.

however, there may be a large proton flux in addition to a low thermal-electron density, which will charge the spacecraft several tens of volts positive. The RTG units, it has been found, do not contribute significantly to charge buildup at any time during a mission to Jupiter or even one to a distance of 10 AU.

The spacecraft equilibrium potential for each region through which the spacecraft would pass is shown in Table 1. These values are given for average condition of solar activity. The potential for near-Earth and near-Jupiter regions varies with the distance from the planet; the values in the table are for 9 planetary radii only. The value given for the interplanetary region will not vary as long as the

Table 1–Summary of regions considered.

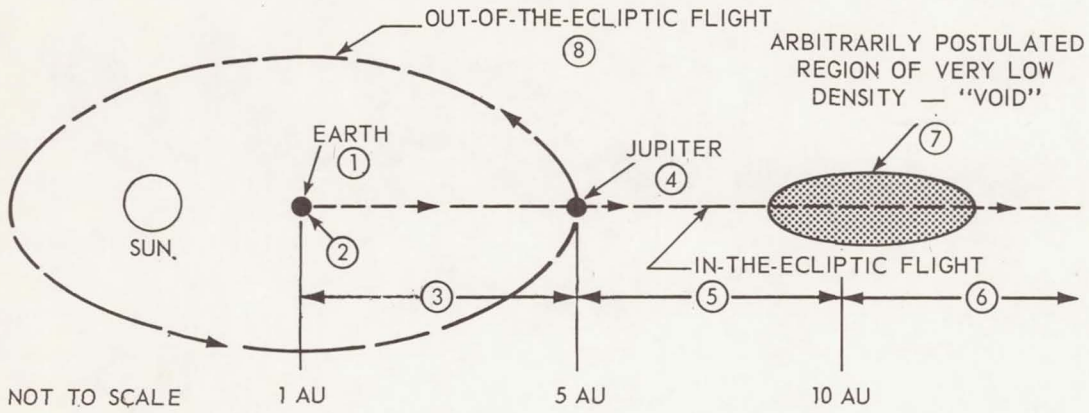

Region	Distance From Sun (AU)	Spacecraft Potential–Average Condition of Solar Activity	Remarks
1. Near-Earth	1	3.5 Volts at 9 R_e	See Figure 9 for Variation of Potential with R_e
2. Earth's Magnetosheath	~1	1.6 Volts	
3. Interplanetary	1 to 5	3.4 Volts	
4. Near-Jupiter	5	26 Volts at 9 R_j	Jupiter Model (Ref. 2) See Table 7 for Variation of Potential with R_j
5. Interplanetary	5 to 10	3.4 Volts	Environment Uncertain, but Extrapolated Based on 1 to 1.5 AU Data
6. Interplanetary	Beyond 10	–	
7. "Void"	–	–	Not Examined in this Task
8. Out-of-the-Ecliptic	–	–	

charged-particle density varies as $1/r_s^2$ and the particle velocity and temperature remain constant. For this report it is assumed that these conditions would be present out to approximately 10 AU.

The influence of the floating potential on possible experiments is briefly discussed in Section V. Experiments designed to measure the thermal electrons or ions could be affected adversely by the spacecraft potential. Therefore, it is necessary that these experiments employ a collector with a large enough dynamic voltage range so that it may sweep the sensor through and appreciably beyond the plasma potential. The effects of the electron sheath that is created by a charged spacecraft must also be considered when one interprets the data. Experiments measuring high-energy particles [i.e., particle energy $(eV) \gg$ spacecraft potential] will not be affected appreciably by the spacecraft potential.

SECTION II

ANALYSIS OF THE CHARGED-PARTICLE ENVIRONMENT

A. Charge Buildup Mechanism—Brief Description

A spacecraft on an interplanetary trajectory is constantly exposed to charged and uncharged particles and to photons. When an encounter occurs, a charge transfer to or from the body will take place. This mechanism of charge transfer can be classified as either charge collection or charge emission. The latter consists of processes such as photoemission, secondary emission (due to impingement of energetic particles on the body), thermal emission, and field emission. Because of the presence of RTG's on the spacecraft another charge emission mechanism is present due to the radioactive materials. The most important processes for the regions of space considered by this Task are the collection of environmental electrons and ions, photoemission, and secondary emission. These mechanisms, as well as RTG emission, are treated in this report. There are other, less important charging mechanisms, which are not treated here, such as cosmic rays, collisions with dust grains, and the previously mentioned thermal and field emission.

A distinction should be made in the charge buildup process between highly energetic particles and lower energy, thermal particles in that the latter are influenced by the spacecraft charge present whereas the former are essentially unaffected by spacecraft charge. It is also noted that the production of electrons by photoemission and secondary emission is dependent on the target material and perhaps even the cleanliness of the material (presence of oxides). Throughout this report, aluminum is assumed to be the exposed material except for the RTG's where beryllium is assumed.

In summary, the rate at which charge buildup proceeds is dependent on the charging or discharging mechanism, the spacecraft materials, and the net charge already present.

B. The Space Environment

The principal energy source of concern in the solar system is the Sun. The Sun is coupled to the environment of the planets through the interplanetary medium. The Sun's varying input to the interplanetary medium and its impact on solar-wind particle radiation and plasma flow is of primary concern. The natural environment and the environment associated with RTG's are treated in this section. It is recognized that particles originating outside the solar system may be of increasing importance to the charge buildup processes as the spacecraft's distance from the Sun increases, but these sources are not considered in this report. Also, areas of extremely low charged-particle density or "voids" have not been postulated or studied in this report.

In evaluating the sources of charge buildup, the regions of near-Earth, near-Jupiter, and interplanetary space are considered separately, as was done in "Radiation Susceptibility Analysis," Task IIA. In this discussion, however, the near-Earth and near-Jupiter regions are each divided into two parts. For the near-Earth region (Figure 1), these are (1) the magnetosphere, which is that region near the Earth where the effect of the Earth's magnetic field on high-energy particles is predominant, and (2) the magnetosheath, which is the transition region between the magnetosphere and interplanetary space. The inner boundary of the magnetosheath is called the magnetopause, and the outer boundary is called the bow shock wave. In this outer boundary region, the particles emanating from the Sun, commonly referred to as the solar wind, are deflected from their normal paths by the magnetic field of the Earth. It is assumed that the near-Jupiter region follows the same pattern as the near-Earth region. Since little is known about the near-Jupiter environment, the available data on the near-Earth particle environment provide useful background information for predicting the environment surrounding Jupiter, although wide variations between these predictions and reality may exist.

1. Earth's Magnetosphere

Two categories of particles in the Earth's magnetosphere are considered. The first category includes the electrons and positive ions that have relatively low (thermal) energies and, therefore, insignificant penetrating capability. The second category includes the high-energy electrons and protons trapped in the Van Allen belt, whose capability of causing radiation damage has been discussed in Task IIA.

The density of thermal electrons in the magnetosphere decreases rapidly with increasing altitude and is strongly dependent on solar activity, which varies periodically ($\sim$11-year cycle) between highly disturbed and relatively quiet conditions. The two curves in Figure 3 show the predicted variations in electron density up to an altitude of 8 R_e (Earth radii) for maximum and minimum conditions of solar activity. These curves are based on recent data published by Gendrin and Haydon and Lucas (Refs. 3 and 4). It should be noted that throughout this report distances referred to in terms of planetary radii are measured from the center of the planet.

The temperature of the thermal electrons is less clearly defined; besides increasing with altitude and being affected by solar activity, it also varies considerably between daytime and nighttime. The matched curves in Figure 4, relating electron temperature to altitude, show the anticipated variation between daytime and nighttime values. They are based on data from Al'pert and Serbu and Maier (Refs. 5 and 6). At 1000 km the values of 1500°K and 3050°K are appropriate for nighttime and daytime, respectively.

The upper curve in Figure 4 (maximum solar activity) in the region above 2.6 R_e is given by Al'pert (Ref. 5) who quotes recent OGO-1 data. Serbu and Maier (Ref. 6) have reported measurements of the electron temperature at radii from 2 to 9 R_e and found a temperature generally less than 22,000°K and a dependence on altitude of the form

$$T_e \propto R_e^b , \tag{1}$$

where b is a number between 1.3 and 3.9. If b is arbitrarily set equal to 2.4 for disturbed conditions of solar activity, then the daytime temperature of 3050°K at 1000 km is in harmony with Al'pert's

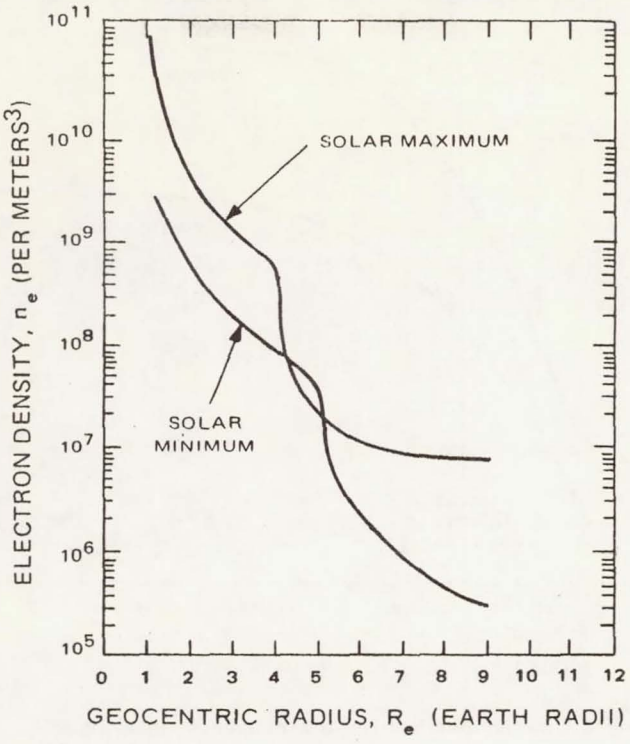

Figure 3—Electron density in the magnetosphere (based on Refs. 3 and 4).

values above 2.6 R_e. In a similar manner, if b is assumed equal to 1.9 for nighttime conditions, then the temperature at 1000 km is in line with the low-temperature data of Serbu and Maier. Therefore, the two curves of Figure 4 obtained in this manner are considered approximate upper and lower limits of electron temperature in the magnetosphere.

Calculations of the omnidirectional thermal-particle flux in the magnetosphere from the data provided in Figures 3 and 4 are based on the expressions

$$\Phi_e = n_e\left(\frac{8kT_e}{\pi m}\right)^{1/2} \tag{2}$$

and

$$\Phi_i = n_i\left(\frac{8kT_i}{\pi M}\right)^{1/2}, \tag{3}$$

where

Φ_e = electron flux,

Φ_i = ion flux,

k = Boltzmann's constant,

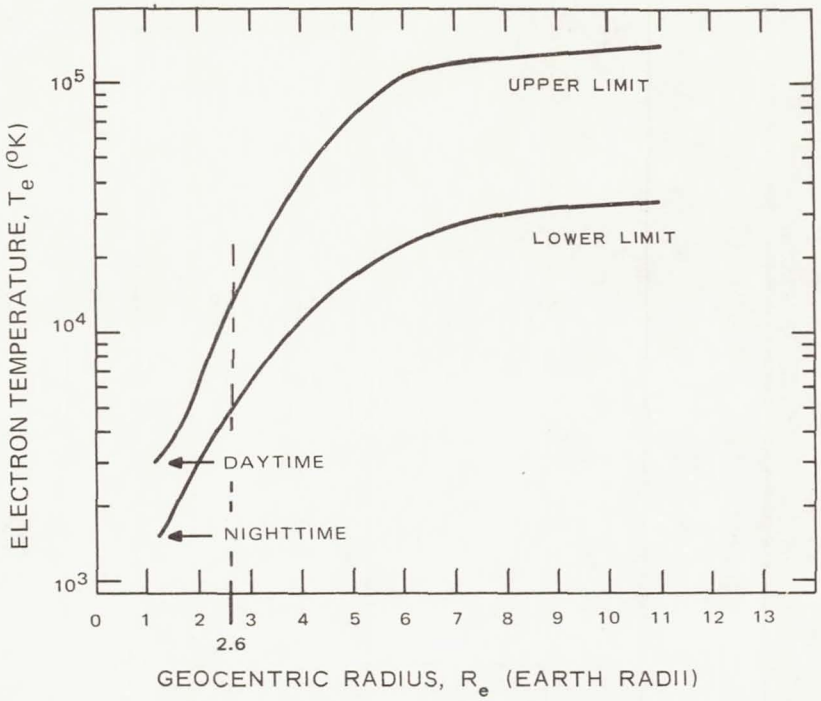

Figure 4—Electron temperature in the magnetosphere (based on Refs. 5 and 6).

n_e = electron density,

n_i = ion density,

T_e = electron temperature,

T_i = ion temperature,

m = electron mass,

and

M = ion mass.

As these expressions indicate, the thermal-particle flux is simply the product of the particle density and the average particle velocity, assuming a Maxwellian distribution. The curves in Figure 5, showing the variation in particle flux with geocentric radius are derived from Figures 3 and 4 with the aid of these equations. The horizontal line indicating photoelectric current density, i_{ph}, has been included in Figure 5 for purposes of comparison that will be discussed in Section III of this report.

In addition to the thermal particles in the magnetosphere, the high-energy electrons and protons trapped in the Van Allen belt may also contribute to the charge buildup process. The curves in Figures 6 and 7, showing trapped electron and proton flux as a function of geocentric radius, were taken from NASA and other publications (Refs. 7 and 8). Information of the same nature was used in estimating the radiation dose resulting from passage of the spacecraft through the Van Allen belt, as discussed in

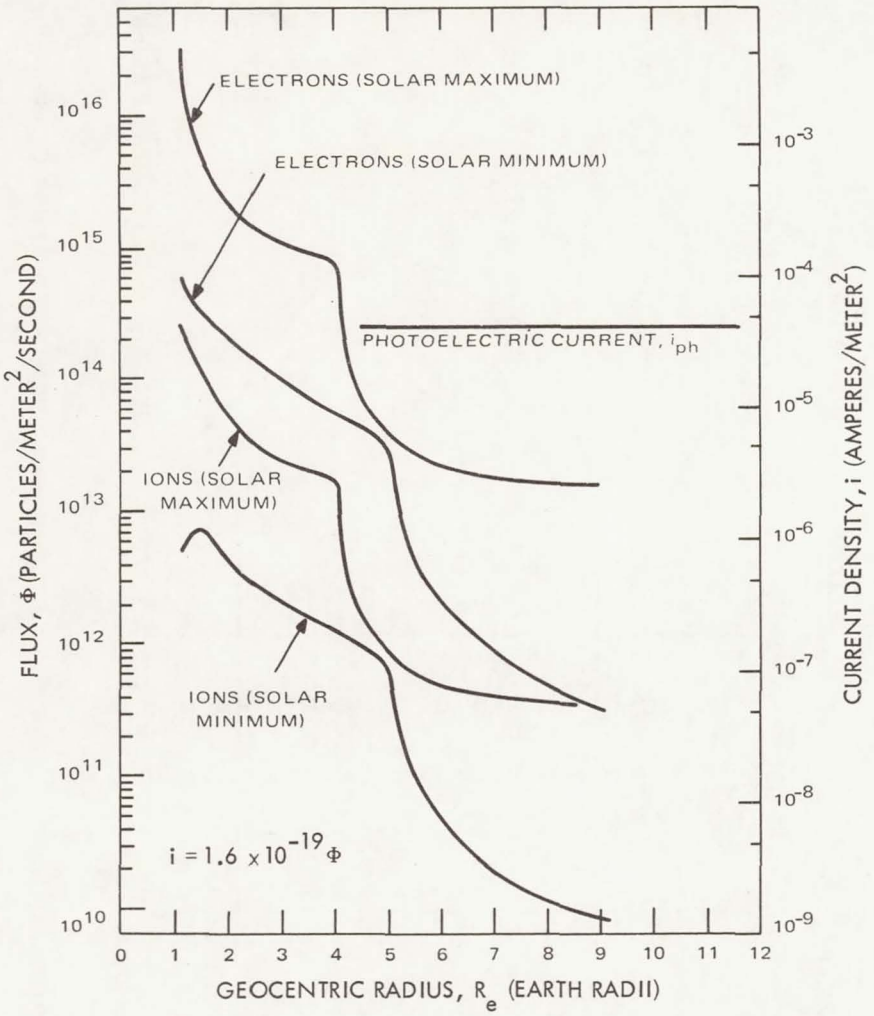

Figure 5—Thermal-electron and ion fluxes in the magnetosphere.

Task IIA. In Figure 6, the two curves show how the trapped electron flux above two different energy levels varies with geocentric radius. Figure 7 provides trapped proton flux data in a similar form. These data are based on averages for a 24-hour period near the plane of the Earth's geomagnetic equator. The current scale in Figures 6 and 7 pertains to a discussion in Section III.

2. Earth's Magnetosheath

In the transition region between the magnetosphere and interplanetary space, the spacecraft will pass through the magnetosheath. Presumably, the spacecraft will penetrate the magnetosheath near the dawn meridian. Estimates of the charged-particle population in this region are available in the literature. The data in Table 2 are based on the model by Spreiter, et al. (Ref. 9), which appears to be in reasonable agreement with actual measurements. The charged particles of principal importance in this region are those that constitute the solar wind. Since the number and energy of charged particles

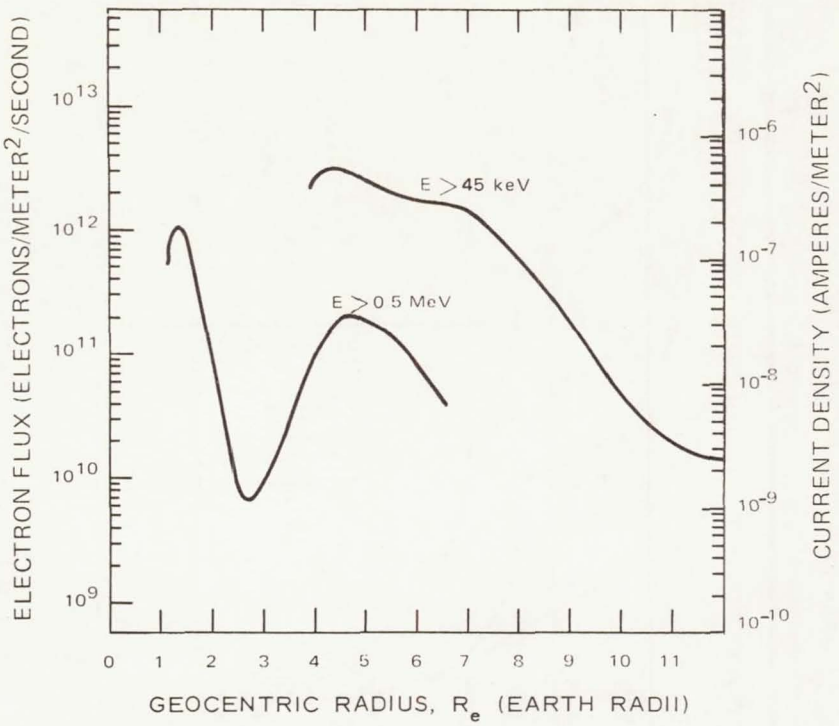

Figure 6—High-energy electron flux in the magnetosphere (Ref. 7).

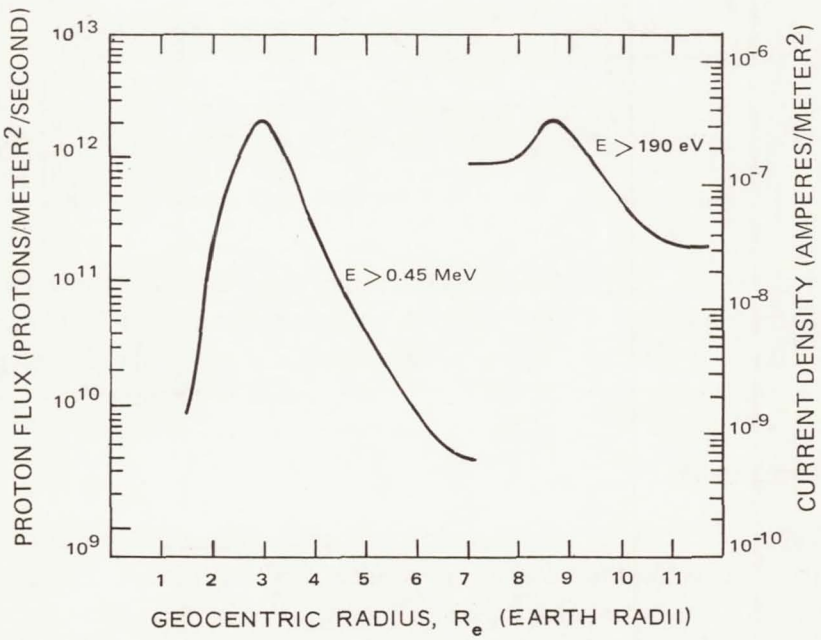

Figure 7—High-energy ion flux in the magnetosphere (Refs. 7 and 8).

Table 2–Parameters in the Earth's magnetosheath and in interplanetary space at 1 AU.

Parameter	Earth's Magnetosheath (Region 2, Table 1)			Interplanetary Space (At 1 AU Within Region 3, Table 1)		
	Minimum	Average	Maximum	Minimum	Average	Maximum
Density, n_e (particles/m^3)	5×10^6	10^7	2.5×10^7	2×10^6	4×10^6	10^7
$T_e = T_i$ (°K)	4.5×10^5	7.5×10^5	1.5×10^6	3×10^4	5×10^4	10^5
Flow Velocity (m/sec)	2.25×10^5	3×10^5	4.5×10^5	3.0×10^5	4×10^5	6.0×10^5

depend on the degree of solar activity, Table 2 provides data for minimum, average, and maximum anticipated conditions.

3. Interplanetary Space

In Table 2, the data for the charged particles in interplanetary space are for the same conditions of solar activity as those in the Earth's magnetosheath and are given for the region just beyond the magnetosheath at a distance of 1 AU. At greater distances from Earth the density is assumed to decrease as $1/r_s^2$, where r_s is the distance from the Sun. The velocity and temperature are assumed to be constant out to the orbit of Jupiter and beyond Jupiter to a distance of 10 AU (Regions 3 and 5, Table 1).

4. Near-Jupiter Environment–Magnetosphere and Magnetosheath

The charged-particle environment in the region near Jupiter is the subject of considerable speculation. The available data are based on observations of radio emissions from the direction of Jupiter at decimeter and decameter wavelengths. Such data provide a rough approximation of the probable extent of the magnetosphere surrounding Jupiter (Ref. 10).

Values of 10 to 30 Gauss for the magnetic field at Jupiter's equatorial surface are based on probable mechanisms for radio emission. From these values and the assumption that the magnetopause of Jupiter is located at the position where the kinetic plasma pressure would equal the magnetic pressure, the location of the magnetopause of Jupiter is estimated to be between 60 and 90 R_j (Jupiter radii). Therefore, the spacecraft trajectory, discussed in Task I, "Mission Analysis," should pass well inside the Jupiter magnetosphere.

The plasma density of the near-Jupiter region, which will greatly affect the charging of the spacecraft, is unknown. Ellis (Ref. 11) has postulated a mechanism for the decameter radio emission from Jupiter and has developed a model for the plasma density in the ionosphere and out to 2 R_j. In a paper that discusses the rotational effects of Jupiter on the distribution of thermal plasma in its magnetosphere, D. B. Melrose (Ref. 12) concluded that in the range of 2.5 to about 8 R_j, the thermal plasma density decreases as $1/R_j^4$. Beyond 8 R_j, the plasma breaks into bunches. For the purpose of

calculation, it is assumed that the plasma density decreases as $1/R_j^4$ beyond 8 R_j and that the density at 2 R_j is 10^9 electrons/m^3 (Ref. 2).

Table 3 gives values for parameters at several planetary radii from Jupiter. The minimum and maximum electron densities are taken simply as 1/5 and 5 times the average density, respectively. Electron and ion temperatures are assumed to be 50,000°K. The column ΩR_j is included, for if the magnetosphere of Jupiter co-rotates with the planet (Ref. 11), then the spacecraft's velocity relative to

Table 3—Near-Jupiter environment parameters.

Radius R_j (Jupiter Radii)	Electron Density Range	Electron Density n_e (particles/m^3)	Particle Velocity* Relative to Spacecraft ΩR_j (m/sec)	Magnetic Field** B (Tesla)
8	Minimum	7.8×10^5	1.0×10^5	2.9×10^{-6}
	Average	3.9×10^6		
	Maximum	2.0×10^7		
9	Minimum	4.9×10^5	1.6×10^5	2.1×10^{-6}
	Average	2.4×10^6		
	Maximum	1.2×10^7		
10	Minimum	3.2×10^5	1.27×10^5	1.5×10^{-6}
	Average	1.6×10^6		
	Maximum	8.0×10^6		
15	Minimum	6.2×10^4	1.9×10^5	4.4×10^{-7}
	Average	3.2×10^5		
	Maximum	1.6×10^6		
20	Minimum	2.0×10^4	2.5×10^5	1.9×10^{-7}
	Average	1.0×10^5		
	Maximum	5.0×10^5		
30	Minimum	4.0×10^3	3.8×10^5	5.6×10^{-8}
	Average	2.0×10^4		
	Maximum	9.9×10^4		
50	Minimum	5.1×10^2	6.3×10^5	1.2×10^{-8}
	Average	2.6×10^3		
	Maximum	1.3×10^4		
Electron temperature T_e = 5×10^4 °K Photoelectric current density i_{ph} = 1.5×10^{-6} A/m^2				

*Ω for Jupiter is 1.76×10^{-4} radians/sec.

**B_0 at 1 R_j is 1.5×10^{-3} Tesla (1 Tesla = 1 Weber/m^2 = 10^4 Gauss).

the rotating plasma will be $(\Omega \times \mathbf{R}_j) + \mathbf{v}'_0$, where $\mathbf{v}'_0$ is the velocity of the spacecraft in a nonrotating frame. The magnetic field has simply been quoted as B_0/R_j^3, where B_0 is the equatorial magnetic field of Jupiter and is taken as 1.5×10^{-3} Teslas.* Magnetic field values for various R_j distances are given in Table 3.

High-energy electrons and protons as well as thermal particles are assumed to be part of the near-Jupiter environment. These high-energy particles, presumably trapped in the magnetic field surrounding Jupiter, may contribute significantly to radiation damage in spacecraft components, as outlined in Task IIA, where the various factors involved in estimating particle population and energy distribution are treated in detail. The principal source of such information for this Task is a recent report by Eggan (Ref. 2). Eggan's report, however, only provides such data over relatively limited energy ranges (0.1 to 4 MeV for protons and 5 to 100 MeV for electrons). Using the Earth's Van Allen belt as a model, estimates were prepared of the trapped protons above 4 MeV and the trapped electrons below 5 MeV, since particles in these energy ranges are of major importance in assessing radiation damage effects (see Task IIA).

In considering charge buildup effects, however, the same assumptions for particle population do not correspond to the possible worst-case condition (i.e., maximum charge buildup). For this reason, calculations of the anticipated charge buildup in the region near Jupiter disregard particles in energy ranges outside those given by Eggan. Under such circumstances, an important source of charge buildup will be the protons in the 0.1 to 4 MeV energy range. At 9 R_j, Eggan's data indicate that the trapped proton flux will be 10^{13} protons/m^2/sec, corresponding to a current density of 1.6×10^{-6} A/m^2. As will be shown in Section III, this current constitutes a possible major source of charge. However, if the extrapolation process used in evaluating radiation damage effects from electrons in the range below 5 MeV is valid, then the effect of the trapped protons in producing charge buildup will be greatly reduced.

C. Other Charging Sources (Excluding RTG's)**

1. Photoemission

Light from the Sun, especially in the UV part of the spectrum, will induce emission of electrons from the spacecraft in sufficient quantity to affect significantly its potential. The emission of electrons from a surface is dependent on the material and on the spectrum of the incident light. In the absence of other charging effects, the resulting potential would be positive. For a body at a negative potential all the emitted electrons will escape, and the current is independent of the potential. To determine the photoelectric current from a body at a positive potential, it is necessary to know the energy spectrum of the emitted electrons. For conditions where the Debye shielding length† is much larger than the spacecraft, the electrons escaping will simply be those with energies greater than the

*1 Tesla = 1 Weber/m^2 = 10^4 Gauss.

**See Paragraph D of Section II for discussion of RTG's.

†Debye length is a characteristic length over which a charged body is shielded; i.e., $L_D = \sqrt{kT_e\epsilon_0/4\pi n_e e^2}$, where ϵ_0 is the permittivity of free space, T_e is the electron temperature, k is Boltzmann's constant, n_e is the number density, and e is the electron charge. Also see *Encyclopedia of Science and Technology* Vol. 10, p. 385. New York: McGraw-Hill Book Co.

potential difference between the spacecraft and the ambient plasma. If the body is large, then the escape of electrons is dependent on the angular distribution of the emitted electrons and the body geometry. Since the Debye length is large at large distances within the Earth's magnetosphere and in interplanetary space, and since the typical deep-space spacecraft has a complex shape, the number of electrons escaping will be taken as that number of electrons with an energy greater than the potential. There have been several measurements of the photoelectron current density in the vicinity of the Earth (Ref. 13). An average value, and the value that will be used for calculations, is 4×10^{-5} A/m^2. In interplanetary space this value will decrease as $1/r_s^2$. The relation between photoelectric current and retarding potential was determined by Hinteregger and Damon (Ref. 14). Fahleson (Ref. 13) states that the spectrum of photoelectrons is approximated by a Maxwellian distribution with a temperature T_{ph} equivalent to 1 eV.

2. Secondary Emission From High-Energy Particle Radiation

To evaluate the contribution to the current density to the spacecraft from high-energy radiation, it is necessary to consider the incident flux and the emission of secondary electrons it produces. The total current density to the body by one component (ions, plus sign; or electrons, minus sign) is

$$i_r = \pm e(\text{incident flux})(1 \pm \delta_{i,e}) , \tag{4}$$

where $\delta_{i,e}$ is the secondary-emission coefficient for ions or electrons. For metals, the electron secondary-emission coefficient for high-energy electron bombardment is not more than 1.7 and is equal to this value only over a small incident electron-energy interval. The maximum secondary-emission coefficient for proton bombardment of aluminum is 4 (Ref. 1).

To determine the secondary-emission current, the integral

$$i_r = e \int_{E_i} f(E_i)[(1 + \delta(E_i)]dE_i , \tag{5}$$

where $f(E_i)$ is the ion energy spectrum, $\delta(E_i)$ is the secondary-electron yield, and E_i is the ion energy, must be evaluated.

The secondary-electron yield function $\delta(E_i)$ is given by Whipple (Ref. 1), and representative ion energy spectra are given in Reference 15. For a spacecraft at a negative potential, this integral is the total current density. For a spacecraft at a positive potential, the energy spectrum of the secondary electrons must be taken into account in a way similar to that employed for the photoelectron energy spectrum.

D. Radiation Environment Induced by RTG's

Radiation emitted by the RTG's consists primarily of neutrons and gamma rays. Neither type of radiation will have a direct effect on the potential of the spacecraft. Interaction of gamma photons with RTG materials and certain spacecraft materials produces electrons. Many of these will have sufficient energy to leave the spacecraft and will therefore tend to cause a positive spacecraft potential.

The electron emission rate was computed for a 75-watt (electrical) RTG.* The maximum gamma flux near the outside of the RTG is about 2.5×10^5 photons/cm^2/sec, computed by the ISOQAD shielding code.** The average photon energy is about 1.5 MeV. The electron generation rate was estimated from the following relation:

$$\Phi_{\gamma,\text{in}} - \Phi_{\gamma,\text{out}} = \Phi_{\gamma,\text{in}}(1 - e^{-\bar{\mu}R}) ,$$

where (see Figure 8)

$\Phi_{\gamma,\text{in}}$ = gamma flux incident on a square centimeter of a beryllium shell (photons/cm^2/sec),

$\Phi_{\gamma,\text{out}}$ = gamma flux transmitted through a square centimeter of a beryllium shell (photons/cm^2/sec),

$\bar{\mu}$ = linear gamma-ray mass absorption coefficient for beryllium (cm^{-1}),

and

R = range of the electrons in beryllium for an average electron energy of 0.75 MeV (cm).

For an incident gamma flux of 2.5×10^5 photons/cm^2/sec, the equation yields

$$\Phi_{\gamma,\text{in}} - \Phi_{\gamma,\text{out}} = 2.4 \times 10^3 \text{ photons/cm}^2\text{/sec} .$$

This represents the number of photons that were involved in Compton scatters within one square centimeter, R centimeters deep. Thus, it is equivalent to an electron generation rate. The probability that the electrons will escape the beryllium is measured by the electron transmission coefficient. The coefficient is about 0.45, based on data in Reference 16. Thus, about $2.4 \times 10^3 \times 0.45$, or 1.1×10^3, electrons/cm^2/sec manage to escape the RTG. If the surface area of the RTG is taken as 5×10^3 cm^2, then the electron emission rate is 5.5×10^6 electrons/sec. Since there are two 75-watt (e) RTG's involved, the total emission rate is of the order of 10^7 electrons/sec. This represents an upper limit since the charge cancellation due to internally generated electrons impinging on the inner surfaces of the RTG was not included. It is not inconceivable that the higher internal gamma fluxes could generate a

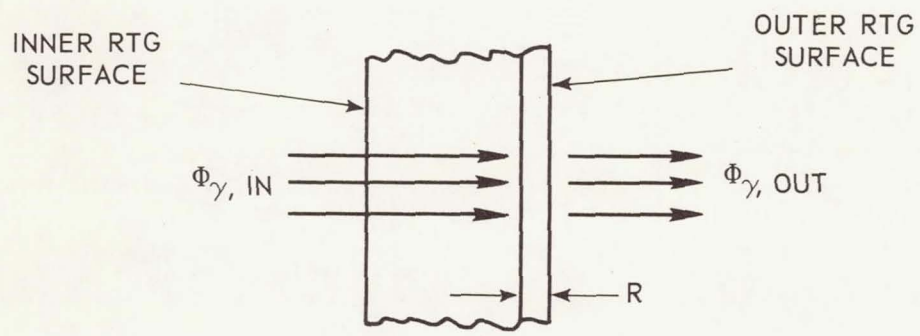

Figure 8—Electron emission model.

*Spacecraft has 2 RTG's, each fueled with PuO_2 isotope of approximately 1725 watts (thermal).

**ISOQAD is a computer program that is used to determine radiation levels, caused by one or several sources of radiation, in one or more energy range, at a point of interest. The program accounts for attenuation, geometric and buildup factors, and intervening materials.

significant number of electrons that would be available for charge cancellation. Analytical evaluation of the electron generation within the RTG is rather involved and was not attempted in this calculation.

The emission rate of 10^7 electrons/sec, which is equivalent to a spacecraft current density* of approximately 1.2×10^{-13} A/m^2, is insignificant compared, for example, with the number of electrons produced by photoemission (see Tables 4 and 5). Therefore, it will have no appreciable effect on spacecraft potential out to the vicinity of Jupiter and beyond Jupiter to a distance of 10 AU. Neutron-induced charged particles are expected to be a second order effect and are not included in this analysis.

* $\frac{\text{emission rate, electrons/sec} \times \text{electron charge}}{\text{assumed surface area of spacecraft, m}^2} = \frac{10^7 \times 1.6 \times 10^{-19}}{4\pi(1)^2} = 1.2 \times 10^{-13}$ A/m^2

SECTION III

CURRENT DENSITY FROM VARIOUS SOURCES

In order to evaluate the relative importance of the various sources of charge buildup, the current densities typical of each source have been calculated. In the Earth's magnetosphere, these densities are directly related to the omnidirectional flux plotted in Figure 5. The current in amperes per square meter is simply 1.6×10^{-19} (the electron charge) times the flux. The anticipated value of the photoelectric current density i_{ph} is also shown in Figure 5.

Current density scales are provided in a similar manner in Figures 6 and 7, which show the variation in high-energy electron and proton flux with altitude within the Earth's magnetosphere.

Current densities typical of the transition region which includes the Earth's magnetosheath and the adjacent interplanetary region at about 1 AU are listed in Table 4. The same table also lists the current density from photoemission which clearly predominates over the other current sources.

Table 5 lists various current densities in the region near Jupiter from the sources discussed in detail in Paragraph IIB-3. Thermal ion current densities were calculated for two conditions: a co-rotating magnetosphere and a nonrotating magnetosphere. The current densities from the high-energy trapped electrons and protons were based on the flux data of Eggan's report (Ref. 2). As indicated previously, no modifications were made to this data to take into account the possibility of encountering trapped electrons with energies below 5 MeV.

Table 4—Near-Earth current densities (A/m^2) for magnetosheath and interplanetary region at 1 AU.

Particle Density Range	Magnetosheath (Region 2, Table 1)		Interplanetary Region		Photoelectric Current Density (i_{ph})
	Electron Current Density	Ion Current Density	Electron Current Density	Ion Current Density	
Minimum	3.3×10^{-6}	2.0×10^{-7}	3.4×10^{-7}	9.6×10^{-8}	
Average	8.6×10^{-6}	5.2×10^{-7}	8.9×10^{-7}	2.5×10^{-7}	4×10^{-5}
Maximum	3.0×10^{-5}	1.9×10^{-6}	3.1×10^{-6}	9.6×10^{-7}	

Table 5–Near-Jupiter current densities (A/m^2).

Radius R_j (Jupiter Radii)	Particle Density Range	Thermal Electrons ($\times 10^{-8}$)	Thermal Ions ($\times 10^{-8}$)		High-Energy Protons ($\times 10^{-8}$)	High-Energy Electrons ($\times 10^{-8}$)
			Co-rotating Magneto-sphere	Nonrotating Magneto-sphere		
	Minimum	17	1.6	0.49		
8	Average	86	7.9	2.4	160	0.016
	Maximum	440	40	13		
	Minimum	10	1.5	0.31		
9	Average	53	7.0	1.5	160	0.032
	Maximum	270	35	7.5		
	Minimum	7.1	0.80	0.20		
10	Average	35	4.0	1.0	32	0.03
	Maximum	180	20	5.0		
	Minimum	1.4	0.20	0.038		
15	Average	7.1	1.0	0.19	–	–
	Maximum	35	5.0	0.95		
	Minimum	0.44	0.17	0.012		
20	Average	2.2	0.85	0.059		
	Maximum	11	4.3	0.29		
	Minimum	0.088	0.026	0.0022		
30	Average	0.44	0.13	0.011		
	Maximum	2.2	0.63	0.055		
	Minimum	0.012	0.0052	0.00030		
50	Average	0.058	0.026	0.0015		
	Maximum	0.29	0.13	0.0075		
Photoelectric current density $i_{ph} = 1.5 \times 10^{-6}$ A/m^2						

An examination of the current-density data indicates that the predominant sources of charge buildup will apparently be the photoemission from the spacecraft and the high-energy protons trapped in the magnetic field around Jupiter. The current density from photoemission decreases rapidly with positive spacecraft potential, whereas the thermal electron current density increases linearly with positive spacecraft potential. The importance of this is shown in the graphical calculation of floating potential V_f that is given in Section IV.

SECTION IV

SPACECRAFT FLOATING POTENTIAL

When the spacecraft reaches an equilibrium, or floating, potential in space, the current emitted from the spacecraft is balanced by the flow of arriving charged particles. Calculations of this potential are based on analytical expressions published by several investigators (Refs. 1, 13, and 17) concerned with the problem of determining the floating potential of a spherical body in a plasma. In such calculations the complex configuration of the spacecraft can be represented by a sphere without introducing significant errors. Other geometric models could have been assumed, but, because of the Debye length it is believed that a sphere is the most accurate. Local effects, such as exposed terminals of a power source (RTG), while not treated here, require special attention for a detailed design of a spacecraft. Whipple (Ref. 1) has presented a comprehensive study of the equilibrium floating potential of a spacecraft together with solutions for the space environment near Earth.

A. Charge Potential Equations

For a stationary conductor in a plasma, the floating potential is simply (Ref. 18):

$$V_f = \frac{kT_e}{2e} \ln\left(\frac{\pi m}{M}\right), \tag{6}$$

where

V_f = the floating potential,

k = Boltzmann's constant,

T_e = the electron temperature,

e = the electron charge,

m = the electron mass,

and

M = the ion mass.

In a plasma with a Maxwellian distribution for the electrons at infinity, the electron current to a sphere at potential ϕ (when ϕ is negative) is

$$I_e = -\pi r^2 Aen\left(\frac{2kT}{\pi m}\right)^{1/2} \exp\left(\frac{e\phi}{kT_e}\right), \tag{7}$$

where

r = the radius of the sphere,

n = the electron (and ion) density,

and

A = a factor such that $1 \leqslant A \leqslant 2$. The factor A accounts for the restriction on electron collection in a magnetic field (Ref. 1); it is further decreased by the reduction of electron collection in the wake of a supersonic body.

The ram ion current due to motion of the spacecraft, neglecting thermal motion, is (Ref. 1, p. 28)

$$I_i = \pi r^2 e n v_0 \left(1 - \frac{2e\phi}{Mv_0^2}\right), \tag{8}$$

where v_0 is the spacecraft velocity.

Sagalyn, et al. (Ref. 19) derived a formula for the ion current (including the effect of thermal motion) that can be approximated by the expression

$$I_i = \pi r^2 n e \left(\frac{8kT_i}{\pi M} + v_0^2\right)^{1/2}. \tag{9}$$

Equations (8) and (9) are combined by substituting

$$\left(\frac{8kT_i}{\pi M} + v_0^2\right)^{1/2}$$

for v_0 in Equation (8) to give

$$I_i = \pi r^2 n e \left(\frac{8kT_i}{\pi M} + v_0^2\right)^{1/2} \left(1 - \frac{2e\phi}{M(8kT_i/\pi M + v_0^2)}\right). \tag{10}$$

When equilibrium is reached, the electron current will, presumably, just balance the ion current at a particular value of potential ϕ called the floating potential V_f. Therefore, the electron current given by Equation (7) can be equated to the ion current given by Equation (10). However, the current resulting from photoemission must also be added to the ion current. If the electron current to the sphere predominates so that the floating potential is negative, then all the electrons generated by the photoelectric effect will escape and this part of the total current will be independent of the potential.

For the negatively charged sphere, equating Equation (7) with Equation (10) and including the photoelectric current gives the following expression for the floating potential:

$$V_f = -\frac{kT_e}{e}\left\{\frac{1}{2}\ln 2A^2 \frac{kT_e}{\pi m} - \ln\left[\left(\frac{8kT_i}{\pi M} + v_0^2\right)^{1/2}\left(1 - \frac{eV_f}{E_i}\right) + \frac{i_{ph}}{ne}\right]\right\}, \tag{11}$$

where E_i is the ion energy

$$\frac{M}{2}\left(\frac{8kT_i}{\pi M} + v_0^2\right)$$

and i_{ph} is the photoelectric current density. Since this equation does not give an explicit solution for V_f, an iterative procedure, implemented by a computer program, must be employed.

If the sphere is charged positively because the ion and photoelectron currents are predominant, then the solution for the floating potential takes a different form. The expression for the thermal electron current becomes

$$I_e = -\pi r^2 Ane\left(\frac{2kT_e}{\pi m}\right)^{1/2}\left(1 + \frac{e\phi}{kT_e}\right). \tag{12}$$

The ion current is given by Equation (10) and the photoelectric current is approximated by

$$I_{ph} = \pi r^2 i_{ph} e \exp\left(\frac{-e\phi}{kT_{ph}}\right), \tag{13}$$

where T_{ph} is taken as 1 eV.

Then the floating potential is given by

$$V_f = -\ln\left\{V_f\left[\frac{1.41Ae}{(\pi mkT_e)^{1/2}} + \frac{2e}{M(8kT_i/\pi M + v_0^2)}\right] - \left(\frac{8kT_i}{\pi M} + v_0^2\right)^{1/2} + A\left(\frac{2kT_e}{\pi m}\right)^{1/2}\right\} + \ln\frac{i_{ph}}{ne}. \tag{14}$$

Again, the term V_f appears in both sides of the equation so that an iterative procedure based on a computer program becomes necessary to obtain a solution in a reasonable length of time.

B. Spacecraft Potential

The considerations and equations developed in Part A of this section and the environmental parameters of Section II are brought together to give the floating potential of a spacecraft in the various environments encountered in the NEW MOONS mission. The equilibrium floating potential, calculated from Equations (11) or (14) for a spherical body in the Earth's magnetosphere, is shown in Figure 9. For the Earth's magnetosheath region and interplanetary space, the floating potential is given in Table 6 for the conditions listed in Table 4. The floating potential in interplanetary space will not vary if the density varies as $1/r_s^2$ and the velocity and temperature remain constant.

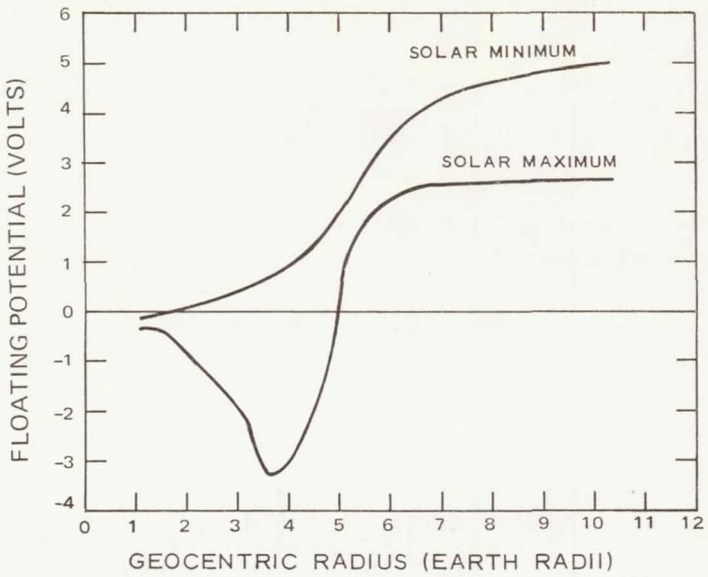

Figure 9—Equilibrium floating potential in the magnetosphere.

Table 6—Spacecraft floating potential (volts) for the Earth's magnetosheath region and interplanetary space.

Particle Density Range	Magnetosheath (Region 2, Table 1)	Interplanetary Space (Regions 3 and 5, Table 1)
Minimum	2.4	4.0
Average	1.6	3.4
Maximum	0.9	2.6

For the near-Jupiter environment, the floating potential is given in Table 7. Column A gives the results of calculations from Equations (11) or (14) for a co-rotating magnetosphere (i.e, $v_0 = \Omega R_j + v'_0$), column B gives the results of calculations for a stationary magnetosphere, and column C lists approximate solutions with the high-energy-proton and secondary-emission currents included.

The equilibrium floating potential for the last case can be determined in a relatively simple manner by a graphical procedure. The individual components of the charging current are plotted separately on the same graph as a function of spacecraft potential. Curves representing the total positive or negative current are obtained by adding the appropriate positive or negative components. The coordinates of the intersection of the total positive and negative current curves, where the two currents are equal, give the equilibrium potential and the currents to the spacecraft. This procedure is illustrated in Figure 10 for a particular set of conditions. The negative current sources are thermal electrons and high-energy electrons. The positive current includes the contributions from thermal protons, high-energy protons, secondary electrons generated by the bombarding protons and by photoemission. In calculating the secondary-emission current, it was assumed that the secondary-emission coefficient for ion bombardment was 2, corresponding to materials that would normally form the outer surface of the

Table 7—Spacecraft floating potential for near-Jupiter environment.

Radius R_j (Jupiter Radii)	Condition Range	Co-rotating Magnetosphere	Stationary Magnetosphere	Approximate Solution*
		A	B	C
8	Minimum	1.9	1.9	81
	Average	0.55	0.48	16
	Maximum	-3.6	-4.1	1.6
9	Minimum	2.3	2.2	129
	Average	0.95	0.87	26
	Maximum	-1.6	-2.2	4.0
10	Minimum	2.7	2.6	80
	Average	1.3	1.2	9.6
	Maximum	-0.10	-0.57	2.4
15	Minimum	4.1	4.0	
	Average	2.7	2.6	
	Maximum	1.3	1.2	
20	Minimum	5.1	5.0	
	Average	3.7	3.6	
	Maximum	2.3	2.2	
30	Minimum	6.7	6.5	
	Average	5.2	5.1	
	Maximum	3.7	3.6	
50	Minimum	8.6	8.3	
	Average	7.1	6.9	
	Maximum	5.6	5.5	

*Includes high-energy-proton and secondary-emission currents based on Jupiter model of Reference 2.

spacecraft, and that the emitted electrons have a Maxwellian distribution with an equivalent temperature of 3.8 eV. The intersection of the positive and negative current indicates that the floating potential will be about 15 volts.

Although the equations for charge collection and floating potential are approximate, and the complex shape of the baseline GJP spacecraft is approximated by a sphere, it is felt that the calculations are reasonably accurate and indicate the importance of the various sources of charge. The effects of the magnetic field are taken into account in regions near the Earth and near Jupiter where the electron gyroradius becomes comparable to or less than the spacecraft dimensions, and in Equations (11) and (14), the factor A is varied appropriately.

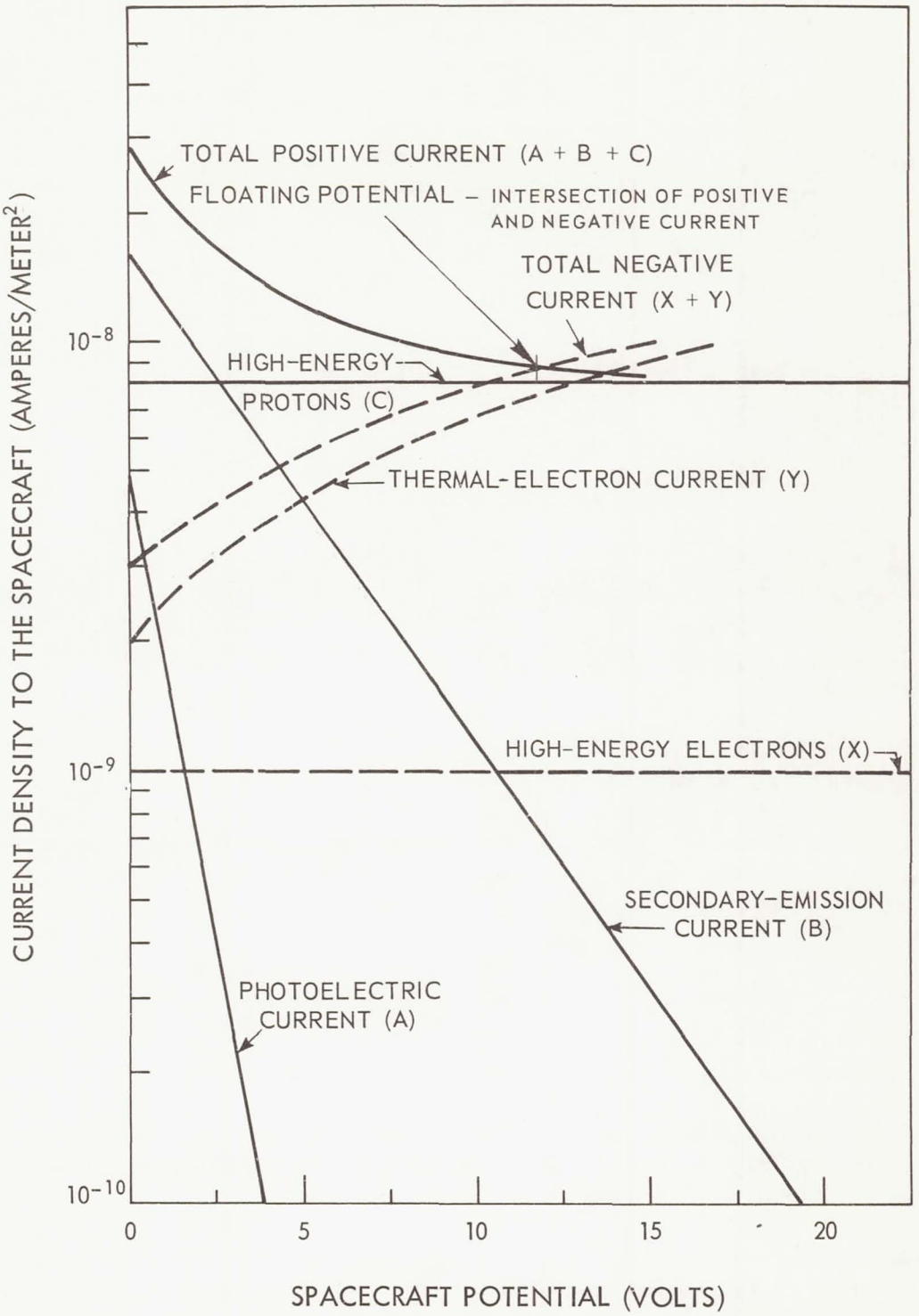

Figure 10—Graphical method to determine the floating potential of a spacecraft in the presence of high-energy radiation—sample calculation at Jupiter.

Note: Spacecraft potential is independent of spacecraft size within the range of the model selected.

SECTION V

PROTECTIVE MEASURES RECOMMENDED FOR CHARGE BUILDUP PROBLEM AREAS

The assumption that the photoelectron spectrum was Maxwellian is only approximately valid. There is a high-energy tail on the energy distribution so that, if the ambient density and electron temperatures are sufficiently low, the higher energy photoelectrons could cause a greater positive spacecraft potential. In laboratory measurements of photoemission, it was found that i_{ph} was an order of magnitude larger for aluminum than for tungsten. However, in experiments with rockets flights, the photoemission from aluminum was found to be of the same order as that from tungsten, and it approximates the value used (Ref. 13). This is probably due to oxidation of the aluminum surface. As the photoelectric density is high in most environments, consideration should be given to reducing the total photoelectric current. For example, if the radio dish antenna were made of mesh rather than solid material, then the photoelectric current would be significantly reduced and the thermal electron collection would be increased. Materials with a high photoelectron yield should be avoided on the sunward side of the spacecraft.

A large flux of high-energy protons (i.e., Eggan's figures) in Jupiter's outer radiation belt is a possible problem if, in addition, the thermal-electron flux is low. However, the energy spectra of the protons and electrons in the Jovian magnetosphere is likely to be similar to that encountered in the Earth's magnetosphere, and consequently there will be a large flux of electrons and protons in the energy range from 200 eV to 40 keV throughout the magnetosphere. This will tend to dominate over the flux of very-high-energy protons and lower the floating potential to a few volts. This is one area that should be investigated more thoroughly.

A vehicle with very long booms moving across a magnetic field will develop an electric field along the booms equal to $\mathbf{v}_0 \times \mathbf{B}$, where $\mathbf{v}_0$ is the vehicle velocity and $\mathbf{B}$ is the magnetic field. If the magnetosphere of Jupiter is co-rotating with the planet, the maximum relative velocity would be 131 km/sec. The magnetic field is 2.2×10^{-6} Teslas, so there would be an electric field of 0.29 V/m. The potential across the GJP booms if the booms are oriented perpendicular to the magnetic field would be about 1.0 volts. The problem of $\mathbf{v}_0 \times \mathbf{B}$ potentials and sheaths has been discussed by Osborne and Kasha (Ref. 20) in relation to the Alouette satellites.

In a discussion of the problems associated with charge collection and vehicle potential, it is necessary to consider the types of experiments that will be affected and what the effects will be. Such spacecraft functions as communication will not be affected by either charge collection or spacecraft potential, and, of course, neither optical nor radio experiments will be affected.

Experiments for measuring high-energy particles [i.e., particle energy (eV) $\gg$ spacecraft potential] will be affected very little by the potential. In experiments to measure, directly, the flux or energy of thermal ions or electrons with Langmuir probes or Faraday-cup probes, the results will be strongly affected by the charge collection and emission, the spacecraft potential, and the sheaths surrounding the spacecraft. Experiments of this type often use the spacecraft potential as a reference, and, therefore, it is necessary to provide the instruments with a sufficient dynamic voltage range so that the sensors may be swept through the plasma potential, several times kT_e/e volts, both positive and negative. The emission of secondary electrons and photoelectrons from the spacecraft creates an electron sheath around the spacecraft, and probes measuring the thermal electrons would detect these secondary and photoelectrons. The problem of sheaths around a moving spacecraft is very complex, and the interpretation of data from low-energy sensors in these sheaths is even more complex (Ref. 21). Resonance RF probes are also affected by the characteristics of the sheath.

SECTION VI

CONCLUSIONS

In the several environments to be encountered by the spacecraft on the NEW MOONS mission considered in this Task, the radiation from the RTG's and associated secondary radiation will not be a major source of charging for the spacecraft. In the environments that have been considered, the spacecraft generally will come to an equilibrium potential that is a few volts positive with respect to the ambient plasma potential. A possible problem would be in the high-energy-proton radiation belts of Jupiter if the proton flux is high, as in Eggan's model, and accompanied by a low flux of thermal electrons.

The effects of a positive floating potential on experiments have been considered. Where the energy range of the particles being measured is much greater than the spacecraft potential, the potential will have little effect on the measurements. The measurement of thermal particles is strongly affected by the spacecraft potential, the charge collection and emission, and the sheath. Therefore, it is necessary to consider all these phenomena in interpreting the data.

Page intentionally left blank

ACKNOWLEDGMENTS

Program

In the course of conducting the studies of the NEW MOONS program, valuable assistance has been provided by many people representing various organizations. It is considered appropriate to identify those whose contributions were most vital.

Fred Schulman, NASA Office of Advanced Research and Technology, and Marcel Aucremann, NASA Office of Space Science and Applications, both realized the necessity for the NEW MOONS studies and provided technical guidance and programmatic support throughout the program.

Daniel G. Mazur, Director of Technology, and Rudolph A. Stampfl, Deputy Director for Advanced Projects, both of Goddard Space Flight Center, aided in program initiation. William S. West directed the NEW MOONS program.

RCA Astro-Electronics Division, the prime contractor, recognized the importance of the NEW MOONS program and has given its support and cooperation toward realizing the objectives of the program. Herbert W. Bilsky was the RCA program manager and technically contributed to the program and provided aid in preparation and review of the manuscripts.

Report Preparation

J. V. Gore and M. A. Kasha of RCA Research Laboratories, Montreal, were the authors of the preliminary draft materials. Bilsky and West, along with Gore and Kasha, prepared the final version of the report. F. J. Osborne, J. A. Nilson, and T. W. Johnston of RCA Research Laboratories provided helpful comments and suggestions in the preparation of this report. K. Campe of Hittman Associates supplied the RTG radiation environment.

Goddard Space Flight Center personnel who have provided important technical information, review, and comments include James H. Trainor, Emil W. Hymowitz, and Joseph H. Conn.

REFERENCES

1. Whipple, E. C., Jr. "The Equilibrium Electric Potential of a Body in the Upper Atmosphere and In Interplanetary Space." NASA Technical Memorandum X-55368, June 1965.
2. Eggan, J. B. "The Trapped Radiation Zones of Jupiter." General Dynamics Report FZM-4789, General Dynamics, Fort Worth Div., Fort Worth, Tex., 1967.
3. Gendrin, R. "Progress Recents dans l'Etude des Ondes T.B.F. et E.B.F." *Space Sci. Rev.* 7: 314-395, 1967.
4. Haydon, G. W., and Lucas, D. L. "Predicting Ionosphere Electron Density Profiles," *Radio Sci.* 3: 111-119, 1968.
5. Al'pert, Ja. L. "On the Outer Ionosphere (and the Transition into Interplanetary Space)." *Space Sci. Rev.* 6: 419-451, 1967.
6. Serbu, G. P., and Maier, E. J. R. "Low Energy Electrons Measured on Imp 2." *J. Geophys. Res.* 71: 3755-3766, 1966.
7. "Significant Achievements in Space Science, 1966." NASA SP-155, 1966.
8. Frank, L. A. "Several Observations of Low Energy Protons and Electrons in the Earth's Magnetosphere with OGO 3." *J. Geophys. Res.* 72: 1905-1916, 1967.
9. Spreiter, J. R., Summers, A. L., and Alksne, A. Y. "Hydromagnetic Flow Around the Magnetosphere." *Planet. Space Sci.* 14: 222-253, 1966.
10. Roberts, J. A. "Jupiter, as Observed at Short Radio Wavelengths." Sympos. on Planetary Atmospheres and Surfaces. *Radio Sci.* 69D: 1543-1552, 1967.
11. Ellis, G. R. "The Decametric Radio Emission of Jupiter." *Radio Sci.* 69D: 1513-1530, 1967.
12. Melrose, D. B. "Rotational Effects on the Distribution of Thermal Plasma in the Magnetosphere of Jupiter." *Planet. Space Sci.* 15: 381-393, 1967.
13. Fahleson, U. "Theory of Electric Field Measurements Conducted in the Magnetosphere with Electric Probes." *Space Sci. Rev.* 7: 238-262, 1968.
14. Hinteregger, H. E., and Damon, K. R. "Analysis of Photoelectrons from Solar Extreme Ultraviolet." *J. Geophys. Res.* 64: 961-969, 1959.
15. White, R. S. "Time Dependence of Low Energy Proton Belts." *J. Geophys. Res.* 72: 943-950, 1967.
16. Magnuson, C. D. and McReynolds, A. W., "Space Electron Radiation Shielding–Bremsstrahlung and Electron Transmission", in "2nd Symposium on Protection Against Radiation in Space" (ed. by Arthur Reetz, Jr.), Washington, D.C., Oct. 12-14, 1964, NASA SP-71, 1965, p. 455.
17. Samir, U., and Willmore, A. P. "The Equilibrium Potential of a Spacecraft in the Ionosphere." *Planet. Space Sci.* 14: 1131-1137, 1966.
18. Chen, F. F. "Plasma Diagnostic Techniques." (ed. by R. H. Huddlestone and S. L. Leonard), New York: Academic Press, 1965, p. 177.
19. Sagalyn, R. C., Smiddy, M., and Wisnia, J. "Measurements and Interpretation of Ion Density Distribution in the Daytime F Region." *J. Geophys. Res.* 68: 199, 1963.
20. Osborne, F. J. F., and Kasha, M. A. "The V × B Interaction of a Satellite with its Environment." *Can. J. Phys.* 45: 263-277, 1967.
21. Medev, D. B. "On the Formation of Satellite Electron Sheaths Resulting from Secondary Emission and Photoeffects", *Interactions of Space Vehicles with an Ionized Atmosphere.* (ed. by S. F. Singer), New York: Pergamon Press, 1965, p. 305.

NASA-Langley, 1971 —— 31